Enhanced Indoor Localization Technique
Based on Point Cloud Conversion Image Matching

Junxian Zhao, He Huang,[*] Dongbo Wang, and Junyang Bian

School of Geomatics and Urban Spatial Information, Beijing University of Civil Engineering and Architecture,
No. 15, Yongyuan Road, Huangcun Town, Daxing District, Beijing 102616, China

It is important that indoor autonomous mobile platforms have the capability of localization in general indoor environments. In this study, using multi-threaded vehicle-mounted light detection and ranging (LiDAR), we conducted indoor autonomous mobile platform localization experiments based on a point cloud conversion 2D image method with an interpolated probability distribution, performed a scan matching analysis by converting 2D images based on an interpolated probability distribution while using occupied grid maps, and introduced a multi-resolution map method to avoid falling into a local optimum. We found that the method adopted in this study achieves a higher indoor positioning accuracy and a higher matching speed with reduced computational effort while avoiding local optima. Compared with other traditional indoor positioning methods, this method has the advantages of universal applicability and robustness against signal interference and other problems.

1. Introduction

Owing to the application and development of technologies based on user location information, positioning technology has become widely used in production and life. However, in indoor environments, such as underground parking lots and indoor parking buildings where autonomous driving may be involved, the accuracy of positioning technology is severely degraded by factors such as building occlusion and multi-path effects and cannot meet the positioning requirements.[1] Indoor environments are characterized by a more serious signal masking than outdoor environments, a limited openness, a stable and orderly layout, a similar composition of indoor structures, and obstacles with regular characteristics. In indoor environments with these characteristics, mobile platforms must select appropriate indoor positioning methods to meet real-time positioning and navigation requirements.

Indoor localization methods can be classified according to technical principles into several types: nearest neighbor method, center of mass localization method, pole method, polygon method, triangulation method, fingerprint method, and trajectory projection method. The nearest neighbor method determines whether the target is within the range of the transmitting

point by the reception of physical signals with range restrictions. The multilateral, polar, and triangulation methods are all rendezvous-based localization methods. Triangulation is used by Wireless Fidelity technology, particularly radar systems. RFID technology relies on the nearest neighbor method for positioning.[2] The positioning accuracy mainly depends on the position and density of the reference label. To achieve higher positioning accuracy, the deployment is usually relatively complicated. Makki *et al.*[3] proposed an important indoor positioning research method that uses wireless device RSSI. The multilateral method determines the location of the target point by measuring the distance from the target point to be measured to a known reference point; in practical applications, the distance estimation is based on the signal arrival time or enhanced observation time difference (E-OTD). Drane *et al.*[4] gave guidance on how to use moving windows to average measurements and reduce signal measurement errors. The method proposed by Drane *et al.* for localization, which combines surrounding mobile calling devices and base stations, is an improvement on the E-OTD method. Faragher and Harle[5] proposed an indoor localization method based on parameters such as how to rapidly attenuate the reception rate of customer broadcasts. Constantinescu[6] used it in emergency call services to find the location of a signal. The triangulation method determines the location of the target point by obtaining the angle between the target point and two known reference points to determine a unique triangle. This method is used in camera-based positioning systems.[7] The fingerprint method establishes a fingerprint map or database by pre-field collection and analysis, after which the signal characteristic parameters that are the closest match to those collected by the device are searched for in the fingerprint database, whose corresponding location is the location of the target. Miyamoto *et al.*[8] proposed a fingerprint method for estimating the user location that employs wireless LAN access points (APs) based on the fingerprint localization method. Mansour *et al.*[9] controlled the pedestrian dead reckoning drift under unconstrained smartphone conditions to improve the pedestrian dead reckoning performance. This approach is based on the trajectory projection method, which essentially determines parameters such as the pedestrian's step length and directional velocity using the known position at the previous moment. The essence of this technique is to determine the parameters of the pedestrian's motion step and directional velocity to obtain the position information at a time when the position is known.

Although these methods can meet indoor positioning requirements in some scenarios, they have shortcomings and defects. The nearest neighbor method must receive signals from the equipment set up in advance, which increases the cost of prearranging scenes and generally reduces location accuracy. The fingerprint method has an excellent localization effect but is difficult to use in the real-time localization system of a complicated indoor environment owing to the huge workload of establishing the fingerprint map in the early stage and the low self-adaptability to the environment. The trajectory projection method is also prone to error accumulation during the operation of the system, which can lead to the reduced robustness and accuracy of the system.

Because laser scanning matching, the core of positioning technology, directly affects the final positioning accuracy, laser point cloud matching methods are mainly divided into point-based and feature-based matching methods. Feature-based matching methods mainly involve the use of point or surface features for matching. Jensfelt and Kristensen proposed a global

scanning matching method based on point features that used corner and edge points,[10] which are more applicable to indoor scenes. The most classical matching method based on line features, the separation and merging algorithm, is a widely adopted line segmentation method.[11] Although this method is simple and efficient, it is only suitable for the scenario of 2D scan matching. Matching methods using point clouds mainly include the iterative closest point method (ICP)[12] and the normal distribution transformation method (NDT).[13] The basic principle of ICP is to determine the corresponding set of nearest points from the set of measured points as a measure of the distance from the set of points to another set of points. Then, a new set of nearest points is formed by calculation, after which an iterative calculation is performed to reduce the distance until a value of the residual sum of squares is satisfied. At this point, the value of the objective function of the residual sum of squares remains unchanged. However, in practical applications, the localization results are inadequate, the matching time is long, and the iterative process may fall into a local optimum.[14]

To develop a method that can be adapted to accurate localization indoors, in this paper, we propose a method that uses an occupancy grid map[15] to represent an arbitrary position of an autonomous mobile platform and performs a map gradient approximation. The method analyzes the effect of the multi-resolution map to perform a series of 3D pose estimation tasks.[16] For the precise localization of the mobile platform itself, any gradient-based method has the risk of falling into a local optimum. To reduce the risk of this occurrence, we carried out experiments employing another method similar to the image pyramid method in computer vision for relevant computations in scan matching, and we generated multi-resolution maps on a high-resolution map without downsampling operations. By converting the 2D image based on the interpolated probability distribution in the case of using the occupancy grid map, we calculated the occupancy probability with sub-grid accuracy, enabling the probability and the largest case in the probability distribution map to be used as a result for scan matching analysis. This approach shortened the matching time and improved the indoor localization of a robot.

2. Point Cloud to 2D Image Conversion

The point cloud data scanned by a multi-line vehicle-mounted light detection and ranging (LiDAR) system carried by a mobile platform is not continuous and must be processed to form a continuous point cloud. The simple pre-processing of a target point cloud, which is generally performed manually, results in an uneven distribution of the point cloud because of the scattered distribution and the effect of the angle of the scanning laser. In the localization experiment based on point cloud image conversion, we used a gradient approximation algorithm that employs an occupancy raster map to represent an arbitrary position of the mobile platform in indoor positioning,[17] where the pitch angle of the mobile platform is almost negligible, owing to the positioning in an indoor corridor.

The cells of a grid map can be seen as a sample distribution of potentially continuous probabilities, and the introduction of a bilinear-filtering-based method of point cloud interpolation calculation allows the estimation of the occupancy probabilities of sub-grid cells. Then, to avoid the risk of falling into a local optimum, according to the experimental results,

multiple occupied grid maps are chosen for use, with each coarser map having half the resolution of the previous one. Also, instead of using a Gaussian filtering method, we generate multiple levels of maps on a high-resolution map, and maps of different resolutions are saved while they are aligned for attitude analysis, ensuring the robustness of the method.

In this experiment, a single frame of a local point cloud was pre-processed and then projected so that the point cloud was in a set 2D plane. The existing point cloud was then processed using a uniform sampling algorithm to produce a uniformly distributed point cloud. On this basis, a local plane coordinate system was established with P_{00} as the origin and P_{01}, P_{10}, and P_{11} forming a unit square that contained an arbitrary serial number continuous coordinate point P_m, as shown in Fig. 1.

In accordance with the above-mentioned rule, $M(P_m)$ is the occupancy probability value at any point P_m, and $M(P_m)$ and the gradient $\nabla M(P_m)$ are calculated from the values at P_{10}, P_{11}, P_{00}, and P_{01}, the four closest points to P_m, as follows:

$$
\begin{aligned}
M(P_m) \approx & \frac{y-y_0}{y_1-y_0}\left(\frac{x-x_0}{x_1-x_0}M(P_{11})+\frac{x_1-x}{x_1-x_0}M(P_{01})\right) \\
& +\frac{y_1-y}{y_1-y_0}\left(\frac{x-x_0}{x_1-x_0}M(P_{10})+\frac{x_1-x}{x_1-x_0}M(P_{00})\right),
\end{aligned}
\tag{1}
$$

$$
\begin{aligned}
\frac{\partial M}{\partial x}(P_m) &\approx \frac{y-y_0}{y_1-y_0}\big(M(P_{11})-M(P_{01})\big)+\frac{y_1-y}{y_1-y_0}\big(M(P_{10})-M(P_{00})\big), \\
\frac{\partial M}{\partial y}(P_m) &\approx \frac{x-x_0}{x_1-x_0}\big(M(P_{11})-M(P_{10})\big)+\frac{x_1-x}{x_1-x_0}\big(M(P_{01})-M(P_{00})\big).
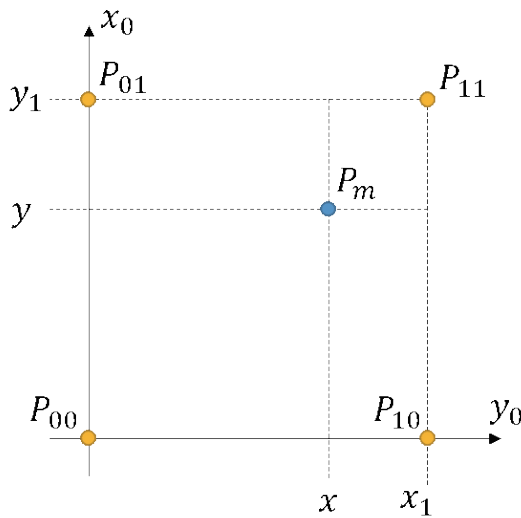\end{aligned}
\tag{2}
$$

Fig. 1.   (Color online) Obtaining occupancy probabilities at any location using interpolation.

Note that the sample points of the map lie within a regular grid owing to the uniform sampling process whereby they are separated from each other by a unit length, which optimizes the gradient approximation equation. From Eq. (2), an approximation can be derived according to the formula.

Any gradient-based calculation runs the risk of falling into a local optimum, and the probability at P_m is interpolated by calculating the gradient. To avoid the risk of falling into a local optimum, we used multi-resolution maps in experiments to overcome and mitigate this risk. Here, our approach was inspired by the image pyramid approach used in computer vision.[18] However, instead of using Gaussian filtering and downsampling, we generated multiple levels of maps on a high-resolution map to obtain a low-resolution map, with each level of resolution being half that of the next, ensuring consistency in the scale of the map.

The maps at all resolutions were obtained from calculations in which the positions of P_m points were controlled, where a sparse distribution of P_m points resulted in low-resolution maps and a dense distribution of P_m points resulted in high-resolution maps. This ensured that the results obtained at different scales reflected the distribution of the continuous probability density, increasing their accuracy. The obtained multi-resolution maps are shown in Fig. 2 in order of raster size (0.1, 0.05, and 0.03 m).

In the experiments, the lowest-resolution map was first matched and then input to the next-highest resolution map by rotating the translation matrix, which was used as the initial state for the next level of scanning and matching. This approach limited the range of matching, thus increasing the speed of the task and reducing the computational burden.

3. Map-matching Method Based on Optimization by Gauss–Newton Method

Matching is a process in which two point clouds of data are continuously scanned and aligned. We use the point of departure of the mobile platform as the origin for matching calculation, and the computed point cloud data must be matched with the point cloud data of the previous frame to achieve the localization of the mobile platform. In our experiment, we used the Gauss–Newton method[19] for the map matching calculation, which is a commonly used method in computer vision. Localization using scan matching generally starts with ICP, a general method for aligning point clouds, but this method is expensive and must be performed in
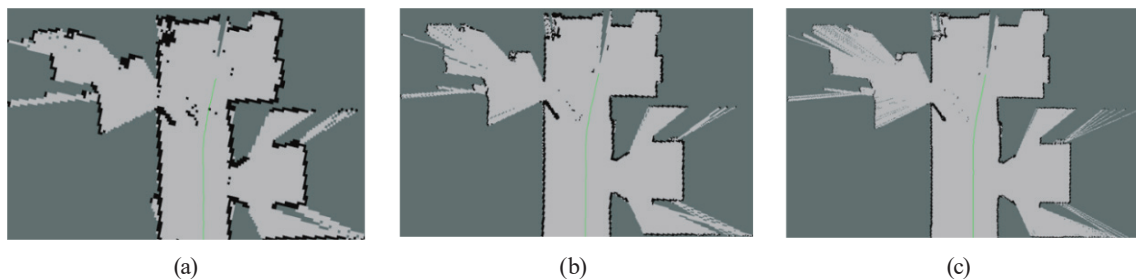

<center>(a)   (b)   (c)</center>

Fig. 2. (Color online) Probability distributions of a point cloud at a location for different resolutions (in order of raster size: (a) 0.1, (b) 0.05, and (c) 0.03 m).

each iteration. The Gauss–Newton method reduces the calculation burden of the system and improves the calculation efficiency while also meeting the requirement of real-time data for the system as much as possible. The Gauss–Newton method is a nonlinear least-squares problem optimization method that can only be used to deal with quadratic functions to achieve data fitting and the optimal estimation of the function. The objective function $F(x)$ is optimized to obtain its minimum value $F(x)_{min}$. In the computational process of this method, an initial value x_0 of x is first given, and then n iterations are performed. In this cycle, the flag is Δx_n. According to the solution of the incremental equation $H\Delta x_n = g$, if Δx_n is sufficiently small to stop the computation and output the value, then the solution of the incremental equation must be computed first. The Hessian matrix is the second derivative of the function, which is equal to $J(x)^T J(x)$. $-J(x)f(x)$ is represented by g. The solution of the incremental equation requires the current Jacobi matrix $J(x_k)$ and its error $f(x_k)$ as the basis for the nth iteration of the computation. Here, x is an n-dimensional variable to be optimized, and $F(x)$ can project this n-dimensional variable to a scalar nonlinear function so that when $F(x)$ achieves the minimum value, $F(x)_{min}$ can be regarded as the optimal solution. The guarantee of a real-time experiment relies on the approximation of the second-order Taylor expansion of the objective function $F(x)$ using the Taylor first-order expansion of the error function $f(x)$ in the Gauss–Newton method.

By using the Gauss–Newton method, the computational burden can be reduced by avoiding the matching calculation of all the corresponding points in the traditional ICP method. We can also reduce the computational burden by continuously scanning the raster map converted into a 2D probability distribution by aligning the reference point cloud and the projection of the source point cloud, and by continuously optimizing until the sum of the probability distributions of all rasters is maximized, as expressed by the following equation:

$$T^* = \operatorname{argmin}\sum_{i=1}^{n}\left[1 - M\left(S_i\left(T\right)\right)\right]^2, \tag{3}$$

where $T = (T_x, T_y, T_\theta)$ denotes the initial position of the vehicle and this matrix is the unit matrix. The maximum value of $M(S_i(T))$ is obtained by minimizing the T^* function, and the sum of the probability distributions of all the grids is maximized. Here, the coordinates of the laser point i after the transformation are represented by $S_i(T)$, and $M(S_i)$ represents the occupancy probability of point S_i in the graph. Note that because the Gauss–Newton method can only solve the least-sum-of-squares problem, it is written as Eq. (4) in the form of a sum of squares to suit the Gauss–Newton method calculation needs. The calculation formula is as follows:

$$S_i\left(T\right) = \begin{bmatrix} \cos T_\theta & -\sin T_\theta & T_x \\ \sin T_\theta & \cos T_\theta & T_y \\ 0 & 0 & 1 \end{bmatrix}\begin{bmatrix} p_{ix} \\ p_{iy} \\ 1 \end{bmatrix}. \tag{4}$$

Because $M(S_i)$ is a nonlinear function of S_i, a first-order Taylor expansion is performed on it as follows:

$$E(T + \Delta T) = \operatorname{argmin}_T \sum \left[1 - M(S_i(T)) - \nabla M(S_i(T)) \frac{\partial S_i(T)}{\partial T} \Delta T \right]^2. \qquad (5)$$

At this time, the equation that minimizes ΔT is then obtained by finding the partial derivative of ΔT and making it equal to 0, as follows:

$$\sum \left[\nabla M(S_i(T)) \frac{\partial S_i(T)}{\partial T} \right]^T \left[1 - M(S_i(T)) - \nabla M(S_i(T)) \frac{\partial S_i(T)}{\partial T} \Delta T \right] = 0. \qquad (6)$$

Therefore, we obtain

$$H = \sum \left[\nabla M(S_i(T)) \frac{\partial S_i(T)}{\partial T} \right]^T \left[\nabla M(S_i(T)) \frac{\partial S_i(T)}{\partial T} \right],$$

$$\Delta T = H^{-1} \sum \left[\nabla M(S_i(T)) \frac{\partial S_i(T)}{\partial T} \right]^T \left[1 - M(S_i(T)) \right]. \qquad (7)$$

Moreover, the gradient $\nabla M(P_m)$ can be approximated using Eq. (2), and from Eq. (4), we obtain

$$\frac{\partial S_i(T)}{\partial T} = \begin{bmatrix} 1 & 0 & -\sin T_\theta * p_{ix} - \cos T_\theta * p_{iy} \\ 0 & 1 & \cos T_\theta * p_{ix} - \sin T_\theta * p_{iy} \end{bmatrix}. \qquad (8)$$

Thus, after performing the above calculations, all values in the incremental equation expressed by Eq. (7) are known, and the transformation matrix ΔT is calculated using the Gauss–Newton method on top of this equation for the iterative solution. The output results can be used to inversely calculate the position coordinates of the robot.

4.   Results

The experiments presented in this study were conducted in a corridor on the second floor of a teaching building in a college, and the state and effect of real-time localization were studied by interpolating the probability-distribution-based 2D image conversion of point clouds based on a single frame of static point cloud data. The length of the corridor was about 70 m and the width was about 3 m, with no large obstacles in the corridor. A HESAI Pandar 40 multi-line vehicle-mounted LiDAR model was used in the experiment, which has a thread count of 40, a scanning frequency of 10/20 Hz, a range accuracy of ±2 cm, an angular resolution of 0.2/0.4°, and a vertical field of view angle between −16 and 7°. The radar and mobile platform used in the experiment are shown in Figs. 3 and 4, respectively. In the experiments, we collected a single frame of point cloud data, which was matched with the previous frame of point cloud data, and

Fig. 3.   (Color online) HESAI Pandar 40 LiDAR.

Fig. 4.   (Color online) Platform for experiments.

the position of the mobile platform was localized in real time by back-calculating the position of the mobile platform in the two frames. Then, the accuracy of the matched results was evaluated and a robustness analysis was performed.

To avoid the risk of this gradient-based approach falling into a local minimum, in this experiment, we used a method inspired by image pyramids in computer vision. However, unlike the image pyramid method, we did not obtain maps with different resolutions by Gaussian blurring or downsampling in the experiment. Instead, we obtained maps by controlling the sparsity of the interpolated points P_m. The resolution is related to the sparsity of P_m; the higher the density, the higher the resolution of the map obtained, and the lower the density, the lower the resolution of the map. As a rule of thumb, the resolution of multi-resolution maps in indoor scenes can be set between 0.03 and 0.5 m. Four matching experiments were conducted with the highest resolution of the cell grid set to 0.03, 0.05, 0.1, and 0.2 m. The matching map-building effects of three of the highest resolutions used in the experiments are shown in Fig. 5.

The map matching results for the three different maximum resolutions are shown in Table 1. The results in the table verify the above-mentioned analysis. At the map resolution of 0.03 m, the matching accuracy RMS has the highest value among the three resolutions, and the corresponding single-frame processing time is also the longest. For the map resolutions of 0.05 and 0.1 m, despite the low matching accuracy, the average single-frame time is shorter than that for the resolution of 0.03 m. Thus, the use of these resolutions can increase the overall speed and robustness of the computation.

However, matching failed for the map with a resolution of 0.2 m in the experiment. The 0.2-m-resolution raster map was very long for the raster length, and the description of the realistic spatial structure details was very vague and inaccurate. Moreover, because the experiment was conducted in a corridor, two sides of the environment were corridor walls, there was a long distance between the ends of the corridor, and there were no highly recognizable markers and references in the environment, which led to a number of mismatched frames. The number of incorrect matches is significantly higher than those of other resolution maps, mainly in map output that does not match the realistic environment significantly, which led to the failure
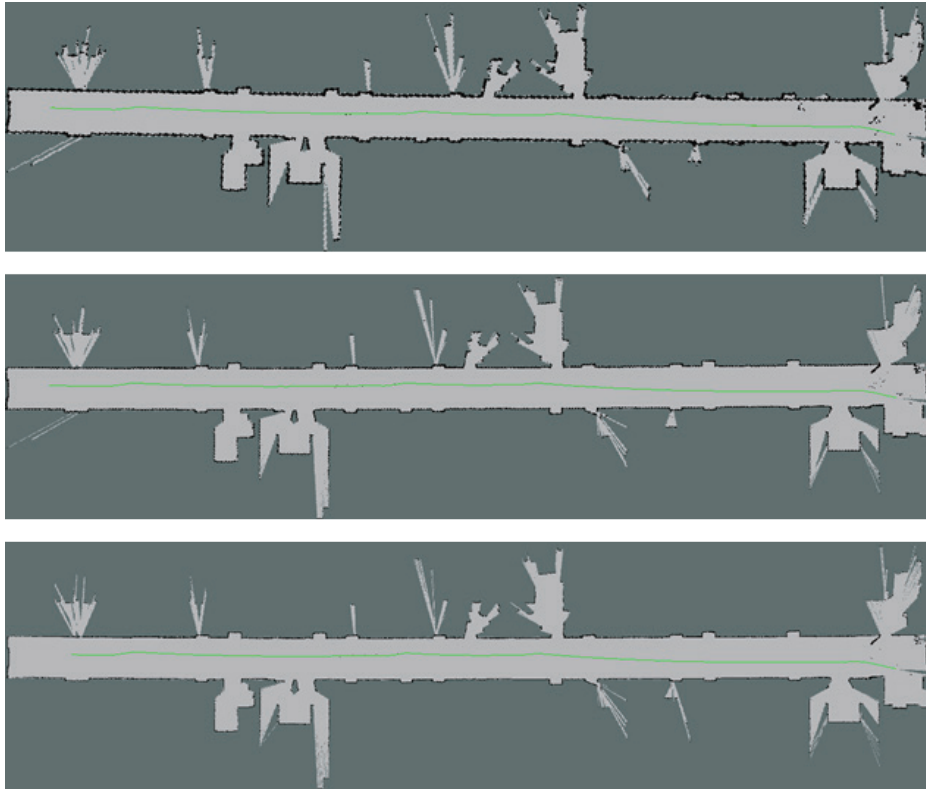
Fig. 5. (Color online) Overall raster plot for three resolutions (top to bottom: 0.1, 0.05, and 0.03).

Table 1
Single-frame matching effects for three different maximum resolutions.

Map resolution (m)	0.03	0.05	0.1
Matching accuracy RMS (correct frame only) (m)	0.08	0.12	0.21
Average time per frame (s)	0.04	0.03	0.02

of matching. The results of matching positioning and the environment map for a resolution of 0.2 m are shown in Fig. 6.

The smaller the raster length, the more detailed the description of the environment in the building and the longer the processing time as the amount of information in the description of the environment increases. Therefore, the use of multi-resolution maps can alleviate the problem of falling into a local optimum, but the use of lower-resolution maps in multi-resolution mapping can also reduce the computational burden and increase the robustness and speed of the matching. They can also be used as initial values for matching under higher-resolution maps. An excessive raster length describes the details inside the building in insufficient detail, leading to a large number of similar structures and the generation of a large number of false matching frames, resulting in the failure of the matching process.

The experimental results indicate that the use of multi-resolution maps for matching localization can avoid the situation of falling into a local optimum due to high-resolution maps
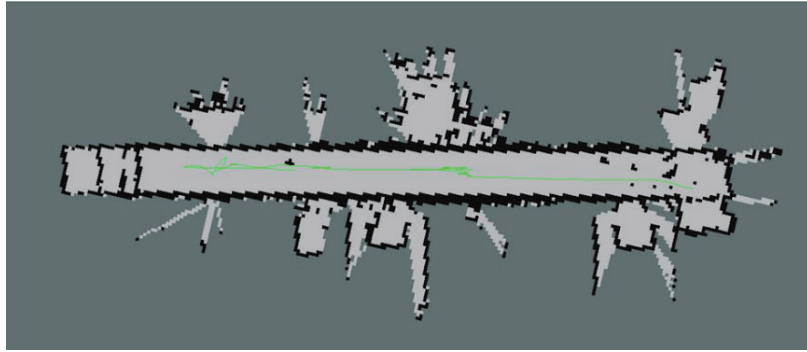
Fig. 6.　　(Color online) Overall raster map at 0.2 m resolution.

Table 2
Comparison of different indoor localization techniques.

Indoor positioning method	WiFi	LiDAR	Ultra wideband	Bluetooth
Accuracy of positioning	5 m	8–21 cm	6–10 cm	1–5 m
Can maps be created?	No	Yes	No	No
Applicable scenarios	Yes	No	Yes	Yes

while considering the accuracy. They also indicate that the adoption of multi-resolution maps is effective in an indoor corridor. Compared with other common indoor positioning technologies, it can establish an accurate map. A comparison of different indoor positioning technologies is shown in Table 2.

5.　Conclusions

Because the conditions of indoor environments are different from those outdoors, for example, the layout of indoor environments is more orderly and regular, to improve the accuracy of mobile platform localization indoors, we developed a method that uses the occupancy grid map method to represent an arbitrary position of a mobile platform and uses the gradient approximation to represent the occupancy grid map. To improve the calculation efficiency and speed of the entire process, we used the Gauss–Newton method in our indoor positioning experiment. To avoid falling into a local optimum, in this study, we used a multi-resolution map method similar to the image pyramid method for matching, which ensures robust, accurate, and high-speed matching. The point cloud conversion image-based method has a higher accuracy than the WiFi positioning method. This method can also establish an indoor map with a similar accuracy to the general UWB and other high-precision positioning methods. Moreover, it can be widely used on mobile platforms such as indoor unmanned dining carts to achieve a stable positioning mobile system that does not require the placement of base stations in the scene and is not subject to signal interference. The proposed method can also be used for indoor environment detection and mapping. However, there were shortcomings in our experiment, such as the use of a single indoor environment (a corridor). There was also no comparison with other indoor

localization methods. Thus, future experiments will be conducted in a variety of different indoor environments, including halls, offices, and underground parking lots. We will also study the impact of different scenes and obstacles on mobile platform matching and positioning, and introduce more indoor positioning methods on this basis. We will compare the advantages and disadvantages of these methods for different situations to achieve higher positioning accuracy and results in specific environments.

References

1 N. B. Vavilova, A. A.Golovan, A. V. Kozlov, and I. A. Papusha: Gyroscopy and Navig. **3** (2021) 12. https://doi.org/10.1134/S207510872103007X.
2 N. Li and B. Becerik-Gerber: Adv. Eng. Inf. **25** (2011) 535. https://doi.org/10.1016/j.aei.2011.02.004
3 A. Makki, A. Siddig, M. Saad, and C. Bleakley: Comput. Networks **88** (2015) 218. https://doi.org/10.1016/j.comnet.2015.06.015
4 C. R. Drane, P. Duffett-Smith, S. Hern, and J. Brice: Location Serv. Navig. Technol. **5084** (2003). https://doi.org/10.1117/12.488154
5 R. Faragher and R. Harle: IEEE J. Sel. Areas Commun. **33** (2015) 2418. https://doi.org/10.1109/JSAC.2015.2430281
6 N.-D. Constantinescu: Rom. J. Inf. Technol. Autom. Control **19** (2009) 1.
7 P. Kemmpi, T. Rautiainen, V. Ranki, F. Belloni, and J. Pajunen: Int. Conf. Indoor Positioning and Indoor Navigation (IEEE, 2010) 1–7. https://doi.org/10.1109/IPIN.2010.5646682.
8 Y. Miyamoto, S. Aikawa, and S. Yamamoto: IEICE Commun. Express **10** (2021) 6. https://doi.org/10.1587/comex.2021XBL0051
9 A Mansour, W. Chen, H. Luo, Y. Li, and J. Wang: Eng. Proc. **10** (2021) 21. https://doi.org/10.3390/ecsa-8-11302
10 P. Jensfelt and S. Kristensen: IEEE Trans. Rob. Autom. **17** (2001) 5. https://doi.org/10.1109/70.964673.
11 S. Liu, M. M. Atia, Y. Gao, and A. Noureldin: Micromachines **6** (2015) 196. https://doi.org/10.3390/mi6020196
12 P. J. Besl and N. D. McKay: Sensor Fusion IV: Control Paradigms and Data Structures **1611** (1992). https://doi.org/10.1117/12.57955
13 S. Bouraine, A. Bougouffa, and O. Azouaoui: Evol. Intell. **15** (2022). https://doi.org/10.1007/s12065-020-00545-y
14 E. Carlsson and J. Carlsson: SN Comput. Sci. **138** (2022) 3. https://doi.org/10.1007/s42979-021-01003-x
15 F. Xu, H. Wang, B. Hua, and M. Ren: Mobile Netw. Appl. **25** (2020) 1496. https://doi.org/10.1007/s11036-019-01378-5
16 J. Yang, Y. Ma, X. Zuo, M. Gong, and L. Cheng: Pattern Recognit. **124** (2022). https://doi.org/10.1016/j.patcog.2021.108439
17 S. Kohlbrecher, O. von Stryk, and J. Meyer: 2011 IEEE Int. Symp. Safety, Security, and Rescue Robotics (IEEE,2011) 155.
18 P. Meer: Comp. Vision, Graphics, and Image Process. **45** (1989) 269. https://doi.org/10.1016/0734-189X(89)90084-4
19 H. Schwetlick: USSR Comput. Math. Math. Phys. **13** (1973) 1. https://doi.org/10.1016/0041-5553(73)90001-3

About the Authors

Junxian Zhao received his B.S. degree from Beijing University of Civil Engineering and Architecture, China, in 2021. He is now studying for his M.S. degree at Beijing University of Civil Engineering and Architecture. His research interests are in semantic SLAM and indoor positioning technology.

He Huang received his B.S. degree from Wuhan University, China, in 2000 and his M.S. and Ph.D. degrees from Sungkyunkwan University, South Korea, in 2004 and 2010, respectively. Since 2010, he has been a lecturer and associate professor at Beijing University of Civil Engineering and Architecture, China. His research interests are in autonomous driving, high-precision navigation maps, and visual navigation and positioning.

Dongbo Wang received his B.S. degree from Shandong University of Technology, China, in 2015 and his M.S. degree from Beijing University of Civil Engineering and Architecture, China, in 2018. Since 2018, he has been working at Planet Map Press, China Rongtong Culture and Education Group Co. His research interests are in high-precision navigation maps and BeiDou navigation and positioning.

Junyang Bian received his B.S. degree from Anhui University of Civil Engineering and Architecture, China, in 2022. He is now studying for his M.S. degree at Beijing University of Civil Engineering and Architecture. His research interests include point cloud semantic segmentation.